Hafnia HfO$_2$ is a proper ferroelectric

Aldo Raeliarijaona [*] and R. E. Cohen [†]

Extreme Materials Initiative, Earth and Planets Laboratory, Carnegie Institution for Science,
5241 Broad Branch Road NW, Washington, District of Columbia 20015, USA

We clarify the nature of hafnia as a proper ferroelectric and show that there is a shallow double well involving a single soft polar mode as in well-known classic ferroelectrics. Using symmetry analysis, density functional theory structural optimizations with and without epitaxial strain, and density functional perturbation theory, we examine several important possible hafnia structures derived ultimately from the cubic fluorite structure, including baddeleyite ($P2_1/c$), tetragonal antiferroelectric $P4_2nmc$, $Pbca$ (nonpolar and brookite), ferroelectric rhombohedral ($R3m$ and $R3$), $Pmn2_1$, and $Pca2_1$ structures. The latter is considered to be the most likely ferroelectric phase seen experimentally and has an antiferroelectric parent with space group $Pbcn$, with a single unstable polar mode and a shallow double well with a well depth of 24 meV/atom. Strain is not required for switching or other ferroelectric properties, nor is coupling of the soft mode with any other modes within the ferroelectric $Pca2_1$, $Pmn2_1$, $R3m$, or $R3$ phases.

I. INTRODUCTION

Hafnia has great potential as a technologically important material due to experimentally observed ferroelectricity in thin films [1,2] and its compatibility with silicon for use in integrated electronics [3,4]. The nature of the observed ferroelectricity is complicated by a complex set of potential phases and distortions from the parent cubic fluorite structure, and by the dependence of its properties and phase relations due to doping, strain, and applied electric fields that give rise to the so-called wake-up effect. Here we clarify that ferroelectric hafnia can be understood as a simple, proper, ferroelectric, from which perturbations from doping, strain, and applied fields can be explored straightforwardly.

Complications in understanding hafnia stem from the fact that there are no known stable ground state polar phases, even varying pressure and temperature [5]. At ambient pressure, the phase diagram shows the fluorite cubic phase ($Fm\bar{3}m$) above 2600 K, tetragonal phase ($P4_2nmc$) between 1800 and 2600 K, and monoclinic baddeleyite ($P2_1/c$) below 1800 K [5]. Increasing pressure at room temperature gives nonpolar orthorhombic $Pbca$ for 5 GPa $\leqslant p \leqslant$ 15 GPa, and $Pnma$ for $p >$ 15 GPa.

It is often mistakenly said that hafnia is an improper ferroelectric [6–8]. This is important, because an improper ferroelectric does not have a normal ferroelectric phase transition. An improper ferroelectric has, by definition, a nonpolar primary order parameter that couples with a polar zone-center mode. If the coupling between the polar mode and the nonpolar mode is even, so that the polar mode can be switched without switching the sign of the coupled mode, an improper

ferroelectric could still be used much as a proper ferroelectric in applications that require ferroelectric switching, but a large peak in dielectric response may not occur near the (nonferroelectric) phase transition.

As we show below, ferroelectric hafnia is a proper ferroelectric with a polar mode giving rise to a symmetric double well. This is true for both the orthorhombic ferroelectrics and the rhombohedral epitaxial hafnia [9]. There is no choice as to what is the proper parent structure to determine whether a ferroelectric is proper or improper. The appropriate parent structure is that of the lowest polarization switching energy under an electric field. It could be a fictive or average structure if the ferroelectric has order-disorder character.

The situation is clear if we compare with well-known classic perovskite ferroelectrics, which are now well understood [10,11]. In the perovskites, the parent paraelectric phase has simple cubic perovskite structure with five atoms per unit cell, but this does not mean that the atoms all sit on their ideal sites. Rather the atoms hop among symmetric off-centered sites, and only the average structure has the simple cubic structure. As the temperature is lowered at ambient pressure, three phase transitions are observed in BaTiO$_3$, for example, cubic to tetragonal ($P4mm$) around 400 K, tetragonal to orthorhombic ($Amm2$) around 280 K, and orthorhombic to rhombohedral ($R3m$) around 200 K [12,13]. However, the transitions are understood to be distortions of the parent *average* structures due to a polar soft phonon, and only the ground state rhombohedral phase is an ordered structure with atoms vibrating around their ideal sites in the $R3m$ structure. In contrast, the classic ferroelectric LiNbO$_3$ has ten atoms per unit cell, from a zone-boundary instability in the parent cubic perovskite. The resulting paraelectric $R\bar{3}c$ phase has a single polar soft mode giving a proper double well to a polar, ferroelectric $R3c$ ground state. Just like in the simple perovskite ferroelectrics,

[*]araeliarijaona@carnegiescience.edu
[†]rcohen@carnegiescience.edu

the atoms do not sit on their ideal sites in the ferroelectric phase, but hop [14,15]. Unlike BaTiO$_3$, etc., in LiNbO$_3$, cubic perovskite never forms below the melting point. As we show below, hafnia is akin to LiNbO$_3$ in that the ferroelectric phase is a proper ferroelectric with a single polar mode, but unlike LiNbO$_3$, at high temperatures the parent tetragonal and cubic phases do form below the melting point, partly due to hafnia's very high melting temperature of 3031 K. Indeed, similar to hafnia, originally Megaw suggested that LiNbO$_3$ switched through the cubic perovskite as its paraelectric parent [16], but Barker and Loudon showed that the parent is $R\bar{3}c$ [17], which was confirmed in later work [14,18].

At high temperatures, cubic fluorite hafnia has a soft zone-boundary mode, X_2^-, leading to tetragonal [6] at 2600 K. However, tetragonal hafnia is dynamically stable with a first-order phase transition to monoclinic baddeleyite at 1800 K. The absence of a polar, stable ferroelectric phase made the discovery of ferroelectricity in thin film hafnia a great surprise [1].

Previous experiments and theory show that ferroelectric hafnia is most likely orthorhombic with space group $Pca2_1$ [19,20]. The energy barriers between ferroelectric $Pca2_1$, the nonpolar ground state baddeleyite $P2_1/c$, orthorhombic antiferroelectric $Pbcn$, and tetragonal antiferroelectric $P4_2nmc$ are all large, larger than $k_B T$ at room temperature for pure hafnia [21]. However, once formed, ferroelectric $Pca2_1$ is metastable and switchable. There have a been a number of proposals for formation of the ferroelectric phase, including doping and vacancies [22], strain [21], kinetics [23], and electric field [24,25]. Other polar phases such as $Pmn2_1$ [26,27] and rhombohedral $R3m$ [9,28] are also metastable albeit with energies larger than that of $Pca2_1$. $Pmn2_1$ has been only proposed theoretically [26,27], whereas $R3m$ has been experimentally observed in (111)-oriented Hf$_{0.5}$Zr$_{0.5}$O$_2$ [9,28]. Reference [29] presented the tree of subgroups from fluorite in hafnia (and zirconia), mostly consistent with our work, though we concentrate on the important phases leading to ferroelectricity, and neglect any phases with partially occupied sites, which are improbable. We concentrate on the symmetry modes (soft and hard modes) over group-subgroup relations. We discuss differences from Nentwich's [29] analysis below in the discussion section.

Cheema *et al.* [30] found that very thin films that are only a couple unit cells thick have an enhanced ferroelectric response and lattice parameters that differ significantly from thicker films or bulk, but we do not address such thin films here using bulk computations. Thicker films of 3–10 nm have lattice parameters consistent with our computations even at zero stress, consistent with previous bulk computations [31,32] and what we report below. Reference [8] considers the large strains in bulk computations, and the authors find that these large strains help promote stability of the ferroelectric $Pca2_1$ phase. Here we show that such large strains are not necessary for ferroelectric behavior, consistent with experimental observations.

In the literature, hafnia has been considered an improper ferroelectric, and several parent structures have been proposed for $Pca2_1$, including fluorite cubic [6], *Ccce* [7], *Pbcm* [33], and tetragonal [8,26]. For ferroelectric $Pmn2_1$, some correctly considered tetragonal $P4_2nmc$ as the parent structure [26,27],

which would be a proper soft-mode transition. Since polar $R3m$ or $R3$ has a higher symmetry than most phases except fluorite cubic and centrosymmetric $R\bar{3}m$ [34], it must have either cubic or rhombohedral as the parent. Reference [6] concluded that ferroelectricity in hafnia is improper and is due to antipolar-polar coupling and nonlinear interactions with the primary phonon instability in cubic X_2^-. In a similar but different way, Zhou *et al.* showed that tensile uniaxial strain and antipolar-polar coupling leads to ferroelectric $Pca2_1$ and claimed that hafnia is an improper ferroelectric [8]. Using a different parent structure, *Ccce* (equivalently, *Bbab*), Ref. [7] claimed that three modes, Γ_{3-}, Y_{3+}, and Y_{2+}, are coupled to generate the $Pca2_1$ structure. In contrast, Ref. [33], using *Pbcm* as the parent structure, stated correctly that ferroelectricity in hafnia is proper, but *Pbcm* is a higher-energy parent, and gives deeper double wells than we show below.

In this paper we clarify symmetry relationships among the different phases of hafnia and the phonon modes that connect them. We find that antiferroelectric *Pbcn* has a zone-center unstable mode Γ_2^-, whose distortion leads to $Pca2_1$. We further find that the double-well potential resulting from this Γ_2^- distortion is shallow, making *Pbcn* key in the polarization switching of $Pca2_1$ hafnia. Having a correct model for hafnia's ferroelectric modes and double wells is important for learning to control its properties by doping, strain, and field, as well for proper understanding of its material physics. In order to optimize its switching behavior and design domain engineering and best epitaxial growth, a correct understanding of the ferroelectric instabilities is crucial.

II. METHODS

We performed symmetry analyses starting with the fluorite structure and the many potential structures from subgroups of the fluorite structure using ISODISTORT [35,36] and the Bilbao Crystallographic Server [37–39]. We performed first-principles calculations using QUANTUM ESPRESSO (QE) [40–42] using Garrity-Bennett-Rabe-Vanderbilt (GBRV) [43] pseudopotentials with the Perdew-Burke-Ernzerhof exchange-correlation functional revised for solids (PBEsol) [44]. We used different exchange-correlation functionals such as the PBE functional [45], but we find that PBEsol gives a volume of baddeleyite in agreement with experimental observation, 1.04% higher than experiment [46]. The plane-wave expansion cutoff energy E_{cutoff} was 544 eV, and the Brillouin zone was sampled using a $6 \times 6 \times 6$ Monkhorst-Pack (MP) grid [47]. Convergence tests were performed for all parameters, and calculations of the depth of the *Pbcn* double well using different MP grids ($4 \times 4 \times 4$ and $8 \times 8 \times 8$) gave similar $\Delta E \simeq 24$ meV/atom. Phonon frequencies were obtained using density functional perturbation theory (DFPT) [48] implemented in the QE PHONON (PH) package [40–42], and the phonon dispersion curves along the Γ–X–M–Γ high-symmetry line of the Brillouin zone (Fig. 3) are an interpolation of the interatomic force constants (IFCs) computed using a $4 \times 4 \times 4$ q-vector grid. The computed energy differences, the relaxed lattice parameters of the various polymorphs, and their Raman spectra compare well with previous studies [49,50].
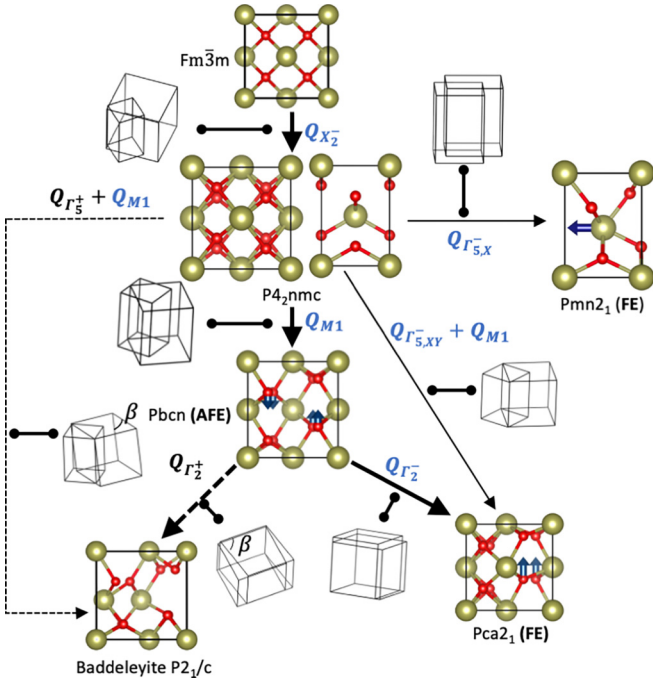
FIG. 1. Summary of the transitions to different hafnia polymorphs starting from cubic fluorite $Fm\bar{3}m$ (topmost) to tetragonal $P4_2nmc$, $Pmn2_1$ (top right), $Pbcn$ (middle), $Pca2_1$ (bottom right), and baddeleyite (bottom left). The symmetry designations of the order parameter responsible for the distortion are labeled near the arrow and are all written in terms of the parent phase (tail of the arrow), as is done throughout this paper. The blue symmetry labels indicate soft modes, and the outlines depict the unit cell relationships. Solid lines with arrows show soft-mode relationships, whereas dashed lines must be first-order transitions. The dark blue arrows on the atoms of the ferroelectric (FE) and antiferroelectric (AFE) structures show the direction of the polarization. The angle β of the monoclinic structure is 99.06°. Not all symmetries shown appear on the phase diagram, nor are all subgroups or pathways shown.

We parametrized the studied distortions using the displacive order parameter Q as the mode amplitude [51]:

$$Q = \sqrt{\sum_i \mathbf{u}_i{}^2},\tag{1}$$

where $\mathbf{u}_i$ is the displacement of atom i in angstroms.

III. RESULTS

A. Group-subgroup relations of different hafnia polymorphs

1. Distortion of fluorite cubic $Fm\bar{3}m$

Firstly, we consider fluorite cubic structure ($Fm\bar{3}m$) because it is the aristotype for hafnia. It has a three-dimensional soft mode X_2^-, whose distortion can be denoted as $Q_{X_{2,i}^-}$, where $i = X, Y$, or Z with a linear combination

$$Q_{X_{2,XYZ}^-} = aQ_{X_{2,X}^-} + bQ_{X_{2,Y}^-} + cQ_{X_{2,Z}^-}\tag{2}$$

denoted by (a, b, c), where a, b, and c are coefficients of the linear combination. The soft X_2^- modes can lead to three possible distortions: $P4_2nmc$ (Fig. 1), $P4/nbm$, and $P\bar{4}3m$. The first two phases are tetragonal distortions of fluorite cubic

TABLE I. Lattice parameters and atomic positions of different $Pbca$ structures. **a**, **b**, and **c** are the crystallographic directions of the orthorhombic Bravais lattice. The atomic positions are given relative to the Bravais lattice vectors. All the atoms sit on Wyckoff position 8c.

	a	**b**	**c**
Pbca nonpolar (this study)			
Lattice parameters (Å)	5.13	5.25	10.07
Atomic positions			
Hf	0.042	0.157	0.862
O	0.169	0.666	0.466
O	0.253	0.589	0.224
Pbca [25]			
Lattice parameters (Å)	5.15	5.29	10.14
Atomic positions			
Hf	0.041	0.343	0.138
O	0.325	0.160	0.032
O	0.248	0.589	0.275
Brookite (this study)			
Lattice parameters (Å)	5.03	9.95	5.20
Atomic positions			
Hf	0.246	0.116	0.536
O	0.002	0.023	0.239
O	0.128	0.710	0.875
Pbca [56]			
Lattice parameters (Å)	5.06	10.02	5.23
Atomic positions			
Hf	0.244	0.385	0.034
O	0.372	0.290	0.372
O	0.000	0.023	0.243

structure according to $(a, 0, 0)$ and $(a, -a, 0)$, respectively. There are possible pathways from $P4/nbm$ to $Pbcn$ or $Pbca$, but we do not explore these further because such pathways have not been observed experimentally to the best of our knowledge. The third possible distortion of X_2^- according to (a, a, a) is $P\bar{4}3m$, which is cubic, noncentrosymmetric and thus piezoelectric, but nonpolar. Interestingly, $P\bar{4}3m$ has been reported in the literature as another possible cubic phase [52–54]. $P\bar{4}3m$ and $P4_2nmc$ have similar powder x-ray diffraction (XRD) patterns with only small differences in the relative intensities. It can therefore be hard to distinguish them in polycrystalline samples.

Two different $Pbca$ structures can be considered a distortion of $Fm\bar{3}m$ (Fig. 2), and they are often confused. They were properly distinguished by Kersch and Falkowski, who called them nonpolar uP61 and antipolar aP61, which is the brookite structure [55]. The designation "OI," as denoted in Ref. [32], is sometimes applied to brookite and sometimes to the nonpolar structure. They have the same Wyckoff positions but different atomic coordinates (Table I and Fig. 2). The o phase in Refs. [25,55] refers to the nonpolar structure, and in Refs. [55,56] to the antipolar brookite. Although brookite might be considered antiferroelectric (Fig. 2), there is no phonon mode that connects it to $Pca2_1$, nor is there a group-subgroup relationship between them. Complicated coupling among six modes plus strain leads to $Pbca$ from cubic, which
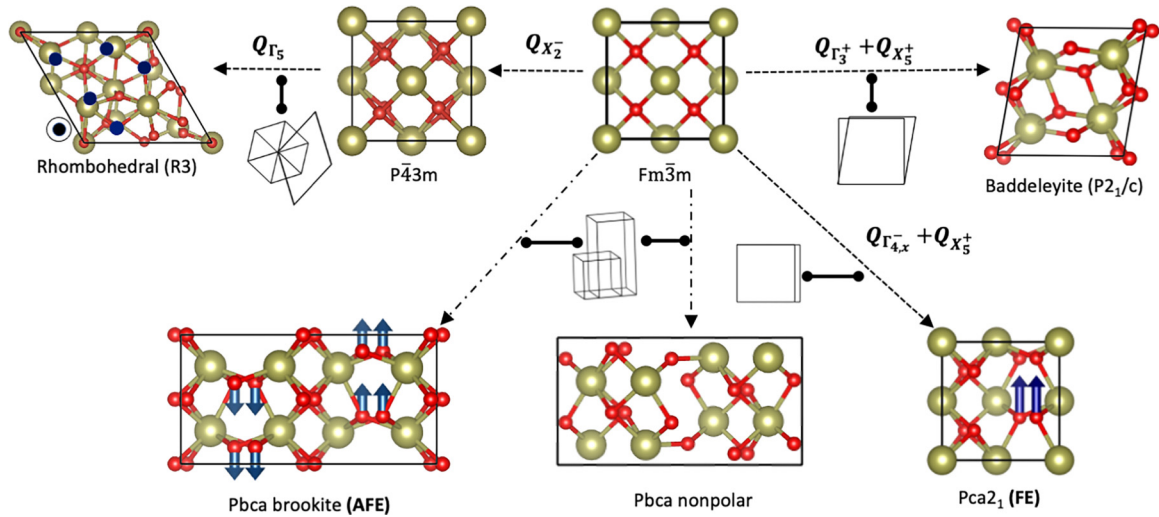
FIG. 2. Summary of the transitions to different hafnia polymorphs starting from cubic fluorite $Fm\bar{3}m$ (center) to rhombohedral $R3m$ (left), $Pca2_1$ (bottom right), orthorhombic $Pbca$ (bottom left), and baddeleyite (right). The symmetry designations of the order parameter responsible for the distortion are labeled near the arrow and are all written in terms of the parent phase (tail of the arrow). The outlines depict the unit cell relationships. The polarization for the rhombohedral phase is out of the page as indicated, along the Cartesian **z** direction. Possible soft-mode transitions are indicated by solid arrows, and possible first-order transitions involving hard modes are all dashed. The dash-dotted lines to the two $Pbca$ structures indicate either a first-order transition from cubic to $Pbca$ or a complicated combination of six optical modes [cubic modes X_5^+, X_5^-, X_3^-, W_3, W_4, and $\Delta_5(0, \frac{1}{2}, 0)$] and strain. Both $Pbca$ structures (brookite antipolar and the nonpolar structure) have the same cubic modes involved in the coupling, but their difference is in their linear combinations. Not all symmetries shown appear on the phase diagram, nor are all subgroups or pathways shown.

would be first order or have intermediate structures (as in Ref. [29]). Coupled distortions (mainly cubic modes X_5^+ and X_3^+) lead to baddeleyite. We stress that in cubic fluorite $Fm\bar{3}m$, the only soft mode is the zone boundary X_2^-. The other distortions of cubic structure, which lead to $Pca2_1$, $Pbca$, and baddeleyite, are all hard modes.

2. Distortion of tetragonal P4₂nmc and Pbcn

The high-temperature tetragonal $P4_2nmc$ phase is also a precursor to antiferroelectric and ferroelectric orthorhombic phases and the ground state baddeleyite. Using group theory, we investigate how baddeleyite, $Pca2_1$, $Pmn2_1$, and $Pbcn$ can be obtained from a transformation of the tetragonal phase.

We find that tetragonal $P4_2nmc$ is related to antiferroelectric $Pbcn$ by a displacive order parameter with $M1$ symmetry (Fig. 1). $M1$ is a soft mode of extensionally strained tetragonal $P4_2nmc$ (see below). $Pca2_1$ is related to tetragonal $P4_2nmc$ through the coupling of the $M1$ and Γ_5^- modes, and baddeleyite results from the coupled $M1$ and Γ_5^+ distortions. We use simplified symmetry designations of the parent structure modes (tetragonal $P4_2nmc$ in this case) according to ISODIS-TORT [35,36]. We found no group-subgroup relation between $Pca2_1$ and baddeleyite, so any transition from ground state baddeleyite to ferroelectric $Pca2_1$ must be through nucleation and growth.

Although not observed experimentally, $Pmn2_1$ is the subject of many computational studies [26,27,52]. Tetragonal $P4_2nmc$ is distorted into the $Pmn2_1$ structure by its $\Gamma_{5,X}^-$ mode (equivalently, $\Gamma_{5,Y}^-$).

$Pbcn$ is a parent of $Pca2_1$ and baddeleyite $P2_1/c$. A distortion of $Pbcn$ with Γ_2^- or Γ_2^+ symmetry generates $Pca2_1$ and

baddeleyite $P2_1/c$, respectively (Fig. 1). The Γ_2^- mode is soft for relaxed $Pbcn$.

There are lots of local minima, which complicates the relationships among the metastable phases. Any of these metastable and saddle point structures might be stabilized entropically with temperature by anharmonic thermal vibrations or hopping.

3. Distortion of cubic P̄43m

Ferroelectricity in hafnia films on hexagonal substrates can also be attributed to polar rhombohedral phases such as $R3m$ or $R3$ [57]. Symmetry investigations indicate that $P\bar{4}3m$ can be distorted into $R3m$ and $R3$ with a single polar mode Γ_4 or Γ_5, respectively, but $P\bar{4}3m$ is lower in total energy than cubic fluorite, as well as the rhombohedral phases ($R3m$, $R3$, and $R\bar{3}m$) for a relaxed lattice. The dynamical instability of the relaxed $P\bar{4}3m$ is a two-dimensional zone-center soft mode that leads to tetragonal $P\bar{4}2m$ and orthorhombic $P222$. Nonetheless, there are conditions under which $P\bar{4}3m$ can become the parent of the polar rhombohedral phases. Under tensile strain (e.g., $a = 5.26$ Å, where a is the cubic lattice constant), a three-dimensional zone-center instability ($T1$) develops in addition to the previously mentioned E mode. One of the $T1$ modes distorts strained $P\bar{4}3m$ into $R3m$, which is more stable by about 6 meV/atom. This indicates that ferroelectricity in rhombohedral hafnia is also proper with a $P\bar{4}3m$ parent structure. The conclusion of improper ferroelectricity in polar rhombohedral hafnia by Ref. [34] is likely because of the use of $R\bar{3}m$ as the parent structure, which is higher in energy than $P\bar{4}3m$.
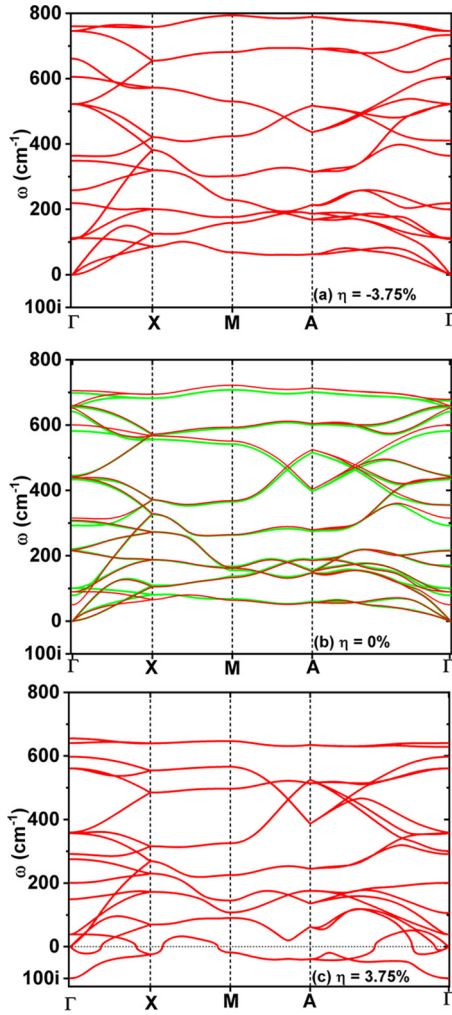
FIG. 3. Phonon dispersion of tetragonal $P4_2nmc$ at strain (a) $\eta = -3.75\%$, (b) $\eta = 0\%$, and (c) $\eta = 3.75\%$. The dotted lines in (c) show the zero frequency level. The epitaxial strain η is a biaxial in-plane strain with c allowed to relax, so that $a_\eta = (1 + \eta)a_0$, where a_0 is the lattice constant of the stress-free tetragonal phase ($a_0 = 5.00$ Å). Shown are the harmonic frequencies, i.e., the square root of the curvature of the potential surface for atoms in their ideal positions. The red and green curves in (b) are the phonon dispersion curves obtained using PBEsol and PBE exchange correlation, respectively.

B. Phonon dispersion

The tetragonal phase is dynamically stable at zero strain and under compressive strain ($0 \leqslant \eta \leqslant -3.75\%$) [Figs. 3(a) and 3(b)]. However, under tensile strain ($\eta \geqslant 2.0\%$ or $a_{\text{epi}} \geqslant 5.13$ Å), tetragonal hafnia becomes unstable. Indeed, for $\eta = 3.75\%$, corresponding to $a_{\text{epi}} = 5.22$ Å [Fig. 3(c)], we find soft modes at the Brillouin zone center (Γ_5^-), the zone-boundary points M ($M1$), X, and A. The lowest branch is soft along the whole M–A–Γ line, indicating the possibility of incommensurate or disordered ferroelectric or antiferroelectric ordering possibly explaining previous observations [6]. Along the A–Γ portion of the phonon dispersion curve around $\omega = 400$ cm^{-1}, we observe avoided crossing of the optical phonon branches. This involves optical branches of the same
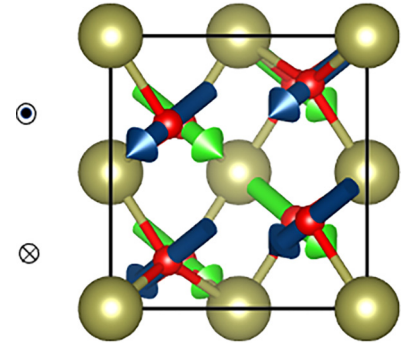

FIG. 4. The arrows show the polar, soft Γ_2^- mode of $Pbcn$ that leads to $Pca2_1$. The $Pbcn$ antipolar direction is top to bottom, and the blue and green arrows indicate displacements of front and back oxygen atoms, respectively. The top oxygen atoms are moving out of the page and the bottom ones are moving into the page as indicated by the symbols adjacent to the structure. $Pca2_1$ can be thought of as polar in one direction (z), and antipolar in the perpendicular x and y directions. The displacements of the hafnium atoms are small in comparison to the oxygen atoms and so are not shown.

symmetry, which tracks back to the E_u at the Γ point. The frequency difference between these two branches decreases as the tensile strain increases, i.e., the strain becomes more positive.

We calculated the phonon dispersion of the relaxed tetragonal phase using PBE and PBEsol [Fig. 3(b)], and they are in excellent agreement. Calculation of the dispersion curves within the local density approximation (LDA) [58] also confirmed the dynamical stability of relaxed $P4_2nmc$. Small quantitative differences are nevertheless found, for example, in the onset of the dynamical instability in the strained tetragonal phase. The first soft mode Γ_5^- is observed around 1.5% tensile strain ($a_{\text{epi}} = 5.05$ Å) when using LDA, but around 2.0% tensile strain ($a_{\text{epi}} = 5.13$ Å) with PBEsol.

C. Soft phonon eigendisplacements

The symmetry mode for the double well in the ferroelectric $Pca2_1$ phase has Γ_2^- symmetry in the antiferroelectric parent $Pbcn$ (Fig. 4). It is an unusual case, though, compared with what one is used to seeing for polar modes in perovskite ferroelectrics. At high temperatures the atoms can hop between the up and down positions in $Pbcn$, which is the tetragonal $P4_2nmc$ $M1$ mode, leading to the tetragonal structure.

The Γ_5^- mode of tetragonal $P4_2nmc$ becomes unstable at 2.0% epitaxial strain ($a_{\text{epi}} = 5.13$ Å). It is a two-dimensional mode, with two symmetrically equivalent displacive order parameters, denoted $Q_{\Gamma_{5,X}^-}$ and $Q_{\Gamma_{5,Y}^-}$, represented as $(a, 0)$ and $(0, a)$, respectively, using ISODISTORT [35,36] notation. We find that the eigendisplacements of the Γ_5^- modes are related by screw symmetry (4_2), i.e., the combination of 90° rotation about the **c** axis followed by a translation by half the lattice constant along the **c** axis (Fig. 5). The distortion of either $Q_{\Gamma_{5,X}^-}$, or $Q_{\Gamma_{5,Y}^-}$ by itself leads to the $Pmn2_1$ ferroelectric phase, and its linear combination

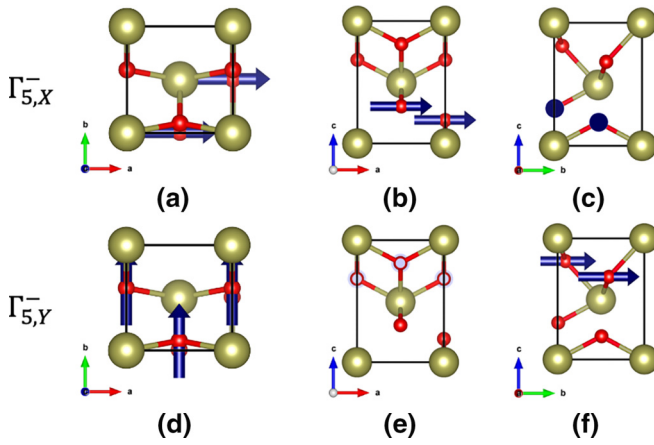$$Q_{\Gamma_{5,XY}^-} = a\,Q_{\Gamma_{5,X}^-} + b\,Q_{\Gamma_{5,Y}^-} \tag{3}$$

FIG. 5. The doubly degenerate Γ_5^- soft modes of tetragonal $P4_2nmc$, denoted by $\Gamma_{5,X}^-$ [(a)–(c)] and $\Gamma_{5,Y}^-$ [(d)–(f)]. The structures were projected on the ab plane [(a) and (d)], ac plane [(b) and (e)], and bc plane [(c) and (f)]. The blue arrows on the atoms indicate the directions of their displacements.

distorts tetragonal $P4_2nmc$ into orthorhombic $Aba2$ when the coefficient $a = b$. $Aba2$ is a saddle point and relaxes to centrosymmetric $Bbab$. $Bbab$ is stable and is 29 meV/atom above baddeleyite in energy.

Pbcn, the centrosymmetric parent of ferroelectric $Pca2_1$, is generated from tetragonal $P4_2nmc$ from the $M1$ distortion (Fig. 1). The order parameter associated with the doubly degenerate soft $M1$ mode is denoted by Q_{M1} and represented as $(a, 0)$, and their eigendisplacements (Fig. 6) are related by 4_2 screw symmetry.

In *Pbcn* the oxygen displacements can be considered as up and down along the antipolar axis (Fig. 7), and the polar mode (Fig. 4) brings one of these displacements (or local polarizations) for half the oxygen atoms in the unit cell to zero, relative to the surrounding hafnia atoms, while the displacement for the other set of oxygens grows to double that in the parent *Pbcn* phase. When the polarization is reversed, the displaced oxygens move to the center of their polyhedra, while the other
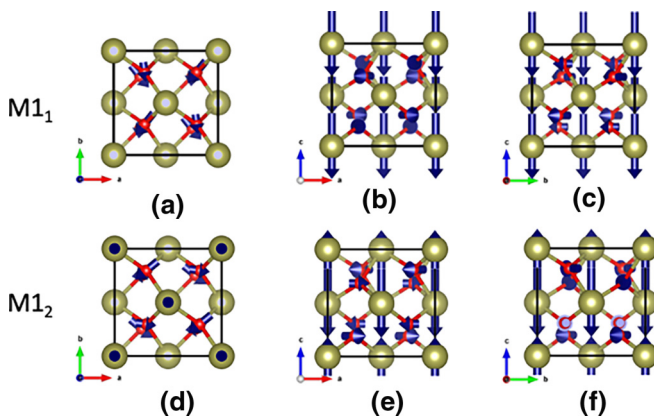

FIG. 6. The doubly degenerate soft $M1$ modes of tetragonal $P4_2nmc$, denoted by $M1_1$ [(a)–(c)] and $M1_2$ [(d)–(f)]. The structures were projected on the ab plane [(a) and (d)], ac plane [(b) and (e)], and bc plane [(c) and (f)]. The blue arrows on the atoms indicate the directions of their displacements.
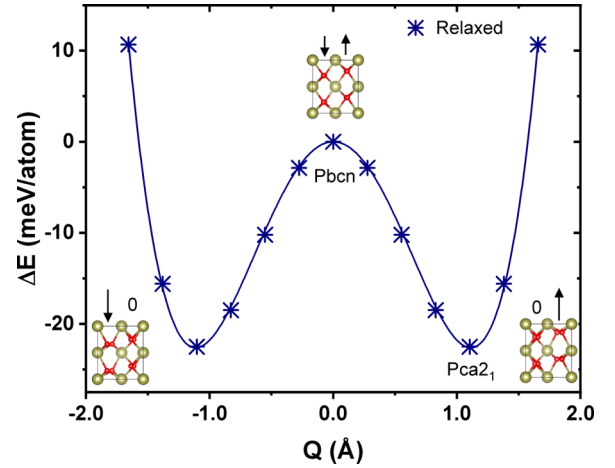

FIG. 7. Potential well for the Γ_2^- symmetry mode leading from *Pbcn* to $Pca2_1$ for a relaxed lattice. The structures corresponding to the three extrema of the double well are drawn above them, and the polarization switching is shown by the polarization configurations: **0** ↑ (right well), ↓↑ (top of double well), and ↓ **0** (left well).

set of oxygens gain a large polarization. So the parent phase has "up, down" polarization, where one side of the double well has "zero, double down" and the other side has "double up, zero." The parent structure can be considered as an ordered antiferroelectric.

For completeness, we also discuss the stabilization of ferroelectric $Pmn2_1$ (Figs. 8 and 9). For an extensional epitaxial strain $\eta \geqslant 2.0\%$ ($a_{epi} \geqslant 5.13$ Å), $Pmn2_1$ is more stable than $P4_2nmc$ along $Q_{\Gamma_{5,X}^-}$.

IV. DISCUSSION

We have shown that there are single polar soft modes that distort the tetragonal and the *Pbcn* parent phases to the polar $Pmn2_1$ and $Pca2_1$ phases, respectively, so that hafnia is a proper ferroelectric. The centrosymmetric parent for the experimentally observed $Pca2_1$ is *Pbcn*, which is dynamically unstable.
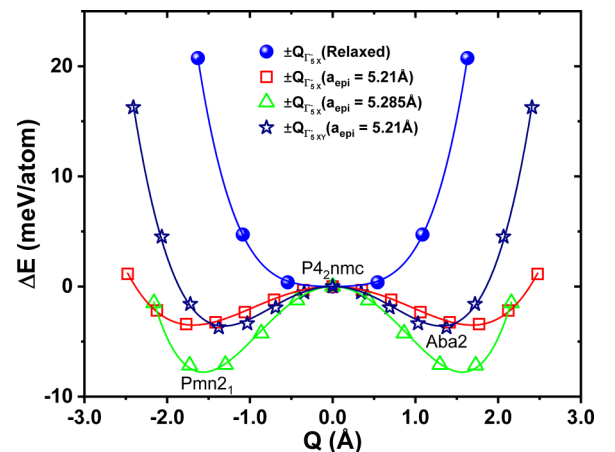

FIG. 8. Energy as a function of $\Gamma_{5,X}^-$ and $\Gamma_{5,XY}^-$ distortions for relaxed tetragonal $P4_2nmc$ (blue curve), for $a_{epi} = 5.21$ Å, and for $a_{epi} = 5.285$ Å.
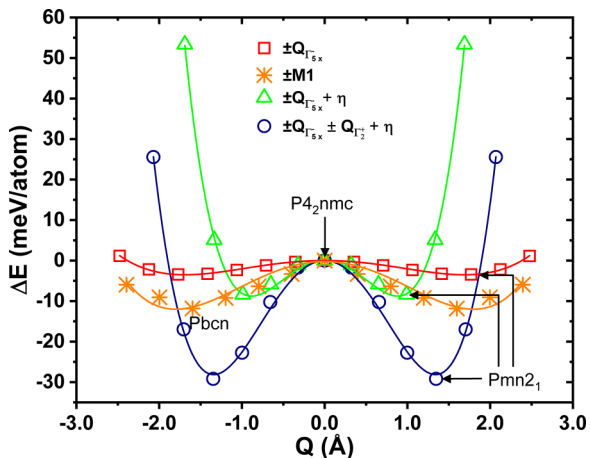
FIG. 9. Energy as a function of distortion for $Pmn2_1$. The curves are labeled according to the irreducible representation, and η indicates that the tetragonal lattice parameters are relaxed. The symmetries of the parent and distorted structure are labeled near the top and bottom of the double well, respectively. The red, green, and blue curves were obtained for $a_\mathrm{epi} = 5.21$ Å, whereas the orange curve was obtained for $a_\mathrm{epi} = 5.25$ Å.

We now consider possible ways to access $Pbcn$ and thus $Pca2_1$, since they are not known to be stable at any conditions of pressure and temperature. Hafnia-based samples are usually annealed at high temperature (>773 K) [59]. Although the temperature-pressure phase diagram of pure hafnia shows that the tetragonal phase is the stable phase at ambient pressure within the temperature range 1800–2600 K [5], the transition temperature usually decreases with doping concentration [22,60], so that the high temperatures (>773 K) used in experiments [59] in doped hafnia are possibly large enough to stabilize the tetragonal phase. The strain imposed by the substrate (e.g., yttria-stabilized zirconia) destabilizes the tetragonal phase, which distorts into $Pbcn$.

Although Ref. [8] indicated $Pbcn$ as a key intermediate phase leading to $Pca2_1$, the parent considered was the tetragonal phase, which led to their conclusion about the improper nature of ferroelectricity in hafnia.

In considering $Pbcm$ as the reference structure instead of cubic, Ref. [33] showed the existence of a single soft polar mode that gives $Pca2_1$, also consistent with proper ferroelectricity in hafnia. $Pbcm$, however, is not a subgroup of the tetragonal phase. The double-well depth from $Pbcn$ to $Pca2_1$ is shallower than $Pbcm$ (72 vs 117 meV/f.u. [33]). The correct switching pathway is the lowest-energy pathway.

The lowest-energy parent structure we find for the ferroelectric $Pca2_1$ phase is $Pbcn$, which is thus the low-energy pathway for switching the polarization direction in hafnia. There may not be a thermodynamically stable phase field for $Pbcn$: that is not required. However, even if formed metastably, it would probably consist of disordered off-centered cells with atoms hopping back and forth between double wells, and have at least partly order-disorder character.

The Bärnighausen tree of the Hf$_x$Zr$_{1-x}$O$_2$ solid solution [29] gives the group-subgroup relations between different hafnia polymorphs. The phases and paths shown there are not complete, since the parent of different structures and the sequence of transitions depends on which mode is first frozen. The fact that Bärnighausen trees are not unique may not have been generally recognized. For example, in the cubic-to-$Pbca$ transition, the freezing of $W3$ or X_3^- distorts the cubic phase into $I4_1/acd$ or $P4/nmm$, which are possible distortions not shown in Ref. [29]. On the other hand, the number of subgroups possible is infinite as pointed out by Bärnighausen [61], so there is always a choice of which to include. Indeed, other possible cubic phases of hafnia can exist such as $P\bar{4}3m$ [52,54]. The latter phase can also be considered a distortion of the aristotype fluorite cubic ($Fm\bar{3}m$). The goal here is to concentrate on low-energy structures and the most probable routes to them from the high-temperature cubic and tetragonal phases. We focus on distortions involving optical phonons and provide physical bases of phase transition through DFT computations. Additionally, the soft phonon modes and the ensuing double-well potential of $Pbcn$ indicate that there is no need for reconstructive transitions as proposed by Ref. [29]. We find that the maximum ion displacements from $Pbcn$ to baddeleyite or $Pca2_1$ are only 0.45 and 0.25 Å, respectively, much smaller than those shown in Ref. [29].

We do not consider disordered phases or static structures with partially occupied sites such as those included in Refs. [29,52] to be likely as static disordered structures are rare in nonmolecular crystals. Common examples in molecular crystals are CO and H$_2$O ice I$_\mathrm{h}$ [62,63]. Disorder in ferroelectrics is more likely to be of a hopping nature, such as in BaTiO$_3$ and KNbO$_3$ [64], where in the eight-site model the atoms hop to give an average cubic structure. $Pbcm$ included in Refs. [29,52] as a parent of $Pbca$ and $Pca2_1$ was refined with half-occupied sites from *in situ* diamond anvil cell x-ray data for ZrO$_2$ [65], but neutron diffraction on quenched samples showed ordered $Pbca$ [66,67].

V. CONCLUSIONS

The number of possible phases, local minima, and saddle points for the ABO_2 (where A and B denote different metallic elements) fluorite aristotype is truly astounding. We have shown the symmetry relations between the high-temperature phases of hafnia and the relevant low-symmetry structures, baddeleyite, $Pca2_1$, $Pmn2_1$, antiferroelectric orthorhombic (AO) $Pbca$, $R3m$, and $Pbcn$. Tetragonal $P4_2nmc$ hafnia is dynamically unstable under tensile strain, and the soft mode $M1$ leads to the antiferroelectric $Pbcn$ structure. $Pbcn$ is the best centrosymmetric parent for ferroelectric $Pca2_1$. Ferroelectricity in hafnia is proper and follows the conventional soft-mode theory. The shallow depth of the $Pbcn$ soft-mode potential well is responsible for polarization switching under applied electric field.

[1] T. S. Böscke, J. Müller, D. Bräuhaus, U. Schröder, and U. Böttger, Ferroelectricity in hafnium oxide thin films, Appl. Phys. Lett. **99**, 102903 (2011).

[2] T. Böscke, J. Müller, D. Brauhaus, U. Schroder, and U. Bottger, *Ferroelectricity in hafnium oxide: CMOS compatible ferroelectric field effect transistors*, in *2011 International Electron Devices Meeting* (IEEE, Piscataway, NJ, 2011), pp. 24.5.1–24.5.4.

[3] J. Robertson, High dielectric constant gate oxides for metal oxide Si transistors, Rep. Prog. Phys. **69**, 327 (2006).

[4] K. J. Hubbard and D. G. Schlom, Thermodynamic stability of binary oxides in contact with silicon, J. Mater. Res. **11**, 2757 (1996).

[5] O. Ohtaka, H. Fukui, T. Kunisada, T. Fujisawa, K. Funakoshi, W. Utsumi, T. Irifune, K. Kuroda, and T. Kikegawa, Phase relations and volume changes of hafnia under high pressure and high temperature, J. Am. Ceram. Soc. **84**, 1369 (2001).

[6] H.-J. Lee, M. Lee, K. Lee, J. Jo, H. Yang, Y. Kim, S. C. Chae, U. Waghmare, and J. H. Lee, Scale-free ferroelectricity induced by flat phonon bands in HfO_2, Science **369**, 1343 (2020).

[7] F. Delodovici, P. Barone, and S. Picozzi, Trilinear-coupling-driven ferroelectricity in HfO_2, Phys. Rev. Mater. **5**, 064405 (2021).

[8] S. Zhou, J. Zhang, and A. M. Rappe, Strain-induced antipolar phase in hafnia stabilizes robust thin-film ferroelectricity, Sci. Adv. **8**, eadd5953 (2022).

[9] Y. Wei, P. Nukala, M. Salverda, S. Matzen, H. J. Zhao, J. Momand, A. S. Everhardt, G. Agnus, G. R. Blake, P. Lecoeur, B. J. Kooi, J. Íñiguez, B. Dkhil, and B. Noheda, A rhombohedral ferroelectric phase in epitaxially strained $Hf_{0.5}Zr_{0.5}O_2$ thin films, Nat. Mater. **17**, 1095 (2018).

[10] R. E. Cohen, Origin of ferroelectricity in perovskite oxides, Nature (London) **358**, 136 (1992).

[11] R. Cohen, Theory of ferroelectrics: a vision for the next decade and beyond, J. Phys. Chem. Solids **61**, 139 (2000).

[12] G. H. Kwei, A. C. Lawson, S. J. L. Billinge, and S. W. Cheong, Structures of the ferroelectric phases of barium titanate, J. Phys. Chem. **97**, 2368 (1993).

[13] T. Ishidate, S. Abe, H. Takahashi, and N. Môri, Phase Diagram of $BaTiO_3$, Phys. Rev. Lett. **78**, 2397 (1997).

[14] I. Inbar and R. E. Cohen, Comparison of the electronic structures and energetics of ferroelectric $LiNbO_3$ and $LiTaO_3$, Phys. Rev. B **53**, 1193 (1996).

[15] H. J. Bakker, S. Hunsche, and H. Kurz, Quantum-mechanical description of the ferroelectric phase transition in $LiTaO_3$, Phys. Rev. B **48**, 9331 (1993).

[16] H. D. Megaw, The thermal expansion of interatomic bonds, illustrated by experimental evidence from certain niobates, Acta Crystallogr. Sect. A **24**, 589 (1968).

[17] A. S. Barker and R. Loudon, Dielectric properties and optical phonons in $LiNbO_3$, Phys. Rev. **158**, 433 (1967).

[18] D. A. Scrymgeour, V. Gopalan, A. Itagi, A. Saxena, and P. J. Swart, Phenomenological theory of a single domain wall in uniaxial trigonal ferroelectrics: Lithium niobate and lithium tantalate, Phys. Rev. B **71**, 184110 (2005).

[19] X. Sang, E. D. Grimley, T. Schenk, U. Schröder, and J. M. LeBeau, On the structural origins of ferroelectricity in HfO_2 thin films, Appl. Phys. Lett. **106**, 162905 (2015).

[20] T. Shimizu, K. Katayama, T. Kiguchi, A. Akama, T. J. Konno, and H. Funakubo, Growth of epitaxial orthorhombic $YO_{1.5}$-substituted HfO_2 thin film, Appl. Phys. Lett. **107**, 032910 (2015).

[21] S. Liu and B. M. Hanrahan, Effects of growth orientations and epitaxial strains on phase stability of HfO_2 thin films, Phys. Rev. Mater. **3**, 054404 (2019).

[22] M. Hoffmann, U. Schroeder, C. Künneth, A. Kersch, S. Starschich, U. Böttger, and T. Mikolajick, Ferroelectric phase transitions in nanoscale HfO_2 films enable giant pyroelectric energy conversion and highly efficient supercapacitors, Nano Energy **18**, 154 (2015).

[23] X. Xu, F.-T. Huang, Y. Qi, S. Singh, K. M. Rabe, D. Obeysekera, J. Yang, M.-W. Chu, and S.-W. Cheong, Kinetically stabilized ferroelectricity in bulk single-crystalline HfO_2:Y, Nat. Mater. **20**, 826 (2021).

[24] R. Batra, T. D. Huan, J. L. Jones, G. Rossetti, Jr., and R. Ramprasad, Factors favoring ferroelectricity in hafnia: A first-principles computational study, J. Phys. Chem. C **121**, 4139 (2017).

[25] R. Materlik, C. Künneth, and A. Kersch, The origin of ferroelectricity in $Hf_{1-x}Zr_xO_2$: A computational investigation and a surface energy model, J. Appl. Phys. **117**, 134109 (2015).

[26] T. D. Huan, V. Sharma, G. A. Rossetti, and R. Ramprasad, Pathways towards ferroelectricity in hafnia, Phys. Rev. B **90**, 064111 (2014).

[27] Y. Qi, S. Singh, C. Lau, F.-T. Huang, X. Xu, F. J. Walker, C. H. Ahn, S.-W. Cheong, and K. M. Rabe, Stabilization of Competing Ferroelectric Phases of HfO_2 under Epitaxial Strain, Phys. Rev. Lett. **125**, 257603 (2020).

[28] N. Kaiser, Y.-J. Song, T. Vogel, E. Piros, T. Kim, P. Schreyer, S. Petzold, R. Valentí, and L. Alff, Crystal and electronic structure of oxygen vacancy stabilized rhombohedral hafnium oxide, ACS Appl. Electron. Mater. **5**, 754 (2023).

[29] M. Nentwich, Structure relations in the family of the solid solution $Hf_xZr_{(1-x)}O_2$, Z. Kristallogr. - Cryst. Mater. **237**, 141 (2022).

[30] S. S. Cheema, D. Kwon, N. Shanker, R. Dos Reis, S. L. Hsu, J. Xiao, H. Zhang, R. Wagner, A. Datar, M. R. McCarter, C. R. Serrao, A. K. Yadav, G. Karbasian, C. H. Hsu, A. J. Tan, L. C. Wang, V. Thakare, X. Zhang, A. Mehta, E. Karapetrova *et al.*, Enhanced ferroelectricity in ultrathin films grown directly on silicon, Nature (London) **580**, 478 (2020).

[31] M. H. Park, H. J. Kim, Y. J. Kim, W. Lee, T. Moon, and C. S. Hwang, Evolution of phases and ferroelectric properties of thin

Hf$_{0.5}$Zr$_{0.5}$O$_2$ films according to the thickness and annealing temperature, Appl. Phys. Lett. **102** (2013).

[32] U. Schroeder, C. Hwang, and H. Funakubo, *Ferroelectricity in Doped Hafnium Oxide: Materials, Properties and Devices*, Woodhead Publishing Series in Electronic and Optical Materials (Elsevier Science, New York, 2019).

[33] H. Aramberri and J. Íñiguez, Theoretical approach to ferroelectricity in hafnia and related materials, arXiv:2302.00688.

[34] W. Ouyang, F. Jia, and W. Ren, Structural stability and polarization analysis of rhombohedral phases of HfO$_2$, arXiv:2306.06018.

[35] H. T. Stokes, D. M. Hatch, B. J. Campbell, and D. E. Tanner, *ISODISPLACE*: a web-based tool for exploring structural distortions, J. Appl. Crystallogr. **39**, 607 (2006).

[36] H. T. Stokes, B. J. Campbell, and D. M. Hatch, ISODISTORT, ISOTROPY Software Suite, https://stokes.byu.edu/iso/isodistort.php.

[37] M. I. Aroyo, A. Kirov, C. Capillas, J. M. Perez-Mato, and H. Wondratschek, Bilbao Crystallographic Server. II. Representations of crystallographic point groups and space groups, Acta Crystallogr. Sect. A **62**, 115 (2006).

[38] M. I. Aroyo, J. M. Perez-Mato, C. Capillas, E. Kroumova, S. Ivantchev, G. Madariaga, A. Kirov, and H. Wondratschek, Bilbao Crystallographic Server: I. Databases and crystallographic computing programs, Z. Kristallogr. - Cryst. Mater. **221**, 15 (2006).

[39] M. I. Aroyo, J. M. Perez-Mato, D. Orobengoa, E. Tasci, G. de la Flor, and A. Kirov, Crystallography online: Bilbao Crystallographic Server, Bulg. Chem. Commun. **43**, 183 (2011).

[40] P. Giannozzi, S. Baroni, N. Bonini, M. Calandra, R. Car, C. Cavazzoni, D. Ceresoli, G. L. Chiarotti, M. Cococcioni, I. Dabo, A. Dal Corso, S. de Gironcoli, S. Fabris, G. Fratesi, R. Gebauer, U. Gerstmann, C. Gougoussis, A. Kokalj, M. Lazzeri, L. Martin-Samos *et al.*, QUANTUM ESPRESSO: a modular and open-source software project for quantum simulations of materials, J. Phys.: Condens. Matter **21**, 395502 (2009).

[41] P Giannozzi, O. Andreussi, T. Brumme, O. Bunau, M. B. Nardelli, M. Calandra, R. Car, C. Cavazzoni, D. Ceresoli, M. Cococcioni, N. Colonna, I. Carnimeo, A. D. Corso, S. de Gironcoli, P. Delugas, R. A. DiStasio, Jr, A. Ferretti, A. Floris, G. Fratesi, G. Fugallo *et al.*, Advanced capabilities for materials modelling with QUANTUM ESPRESSO, J. Phys.: Condens. Matter **29**, 465901 (2017).

[42] P. Giannozzi, O. Baseggio, P. Bonfá, D. Brunato, R. Car, I. Carnimeo, C. Cavazzoni, S. de Gironcoli, P. Delugas, F. Ferrari Ruffino, A. Ferretti, N. Marzari, I. Timrov, A. Urru, and S. Baroni, QUANTUM ESPRESSO toward the exascale, J. Chem. Phys. **152**, 154105 (2020).

[43] K. F. Garrity, J. W. Bennett, K. M. Rabe, and D. Vanderbilt, Pseudopotentials for high-throughput DFT calculations, Comput. Mater. Sci. **81**, 446 (2014).

[44] J. P. Perdew, A. Ruzsinszky, G. I. Csonka, O. A. Vydrov, G. E. Scuseria, L. A. Constantin, X. Zhou, and K. Burke, Restoring the Density-Gradient Expansion for Exchange in Solids and Surfaces, Phys. Rev. Lett. **100**, 136406 (2008).

[45] J. P. Perdew, K. Burke, and M. Ernzerhof, Generalized Gradient Approximation Made Simple, Phys. Rev. Lett. **77**, 3865 (1996).

[46] S. Pathak, P. Das, T. Das, G. Mandal, B. Joseph, M. Sahu, S. D. Kaushik, and V. Siruguri, Crystal structure of monoclinic hafnia (HfO$_2$) revisited with synchrotron X-ray, neutron diffraction and first-principles calculations, Acta Crystallogr. Sect. C **76**, 1034 (2020).

[47] H. J. Monkhorst and J. D. Pack, Special points for Brillouin-zone integrations, Phys. Rev. B **13**, 5188 (1976).

[48] S. Baroni, S. de Gironcoli, A. Dal Corso, and P. Giannozzi, Phonons and related crystal properties from density-functional perturbation theory, Rev. Mod. Phys. **73**, 515 (2001).

[49] A. Raeliarijaona and R. E. Cohen, First-principles calculations of Raman and infrared spectroscopy for phase identification and strain calibration of hafnia, Appl. Phys. Lett. **120**, 242903 (2022).

[50] A. Raeliarijaona and R. E. Cohen, Origin of wake-up effect in hafnia, arXiv:2302.01981.

[51] The normal mode amplitude is "the square root of the sum of the squares of the mode-induced changes within the primitive supercell (i.e. the root-summed-squared displacement...)" [H. T. Stokes, B. J. Campbell, and D. M. Hatch, ISODISTORT help, https://stokes.byu.edu/iso/isodistorthelp.php].

[52] S. V. Barabash, Prediction of new metastable HfO$_2$: toward understanding ferro- and antiferroelectric films, J. Comput. Electron. **16**, 1227 (2017).

[53] C. Wang, S. Azad, S. Thevuthasan, V. Shutthanandan, D. McCready, and C. Peden, Distortion of the oxygen sublattice in pure cubic-ZrO$_2$, J. Mater. Res. **19**, 1315 (2004).

[54] S. Bichelmaier, J. Carrete, R. Wanzenböck, F. Buchner, and G. K. H. Madsen, Neural-network-backed effective harmonic potential study of the ambient pressure phases of hafnia, Phys. Rev. B **107**, 184111 (2023).

[55] A. Kersch and M. Falkowski, New low-energy crystal structures in ZrO$_2$ and HfO$_2$, Phys. Status Solidi **15**, 2100074 (2021).

[56] O. Ohtaka, T. Yamanaka, S. Kume, N. Hara, H. Asano, and F. Izumi, Structural analysis of orthorhombic hafnia by neutron powder diffraction, J. Am. Ceram. Soc. **78**, 233 (1995).

[57] B. Noheda and J. Íñiguez, A key piece of the ferroelectric hafnia puzzle, Science **369**, 1300 (2020).

[58] J. P. Perdew and A. Zunger, Self-interaction correction to density-functional approximations for many-electron systems, Phys. Rev. B **23**, 5048 (1981).

[59] H. Joh, M. Jung, J. Hwang, Y. Goh, T. Jung, and S. Jeon, Flexible ferroelectric hafnia-based synaptic transistor by focused-microwave annealing, ACS Appl. Mater. Interfaces **14**, 1326 (2022).

[60] M. H. Park, T. Schenk, M. Hoffmann, S. Knebel, J. Gärtner, T. Mikolajick, and U. Schroeder, Effect of acceptor doping on phase transitions of HfO$_2$ thin films for energy-related applications, Nano Energy **36**, 381 (2017).

[61] H. Bärnighausen, Group-subgroup relations between space groups: a useful tool in crystal chemistry, MATCH: Commun. Math. Chem. **9**, 139 (1980).

[62] J. O. Clayton and W. F. Giauque, The heat capacity and entropy of carbon monoxide. Heat of vaporization. Vapor pressures of solid and liquid. Free energy to 5000°K. From spectroscopic data, J. Am. Chem. Soc. **54**, 2610 (1932).

[63] L. Pauling, The structure and entropy of ice and of other crystals with some randomness of atomic arrangement, J. Am. Chem. Soc. **57**, 2680 (1935).

[64] R. Comès, M. Lambert, and A. Guinier, Désordre linéaire dans les cristaux (cas du silicium, du quartz, et des pérovskites ferroélectriques), Acta Crystallogr. Sect. A **26**, 244 (1970).

[65] Y. Kudoh, H. Takeda, and H. Arashi, In situ determination of crystal structure for high pressure phase of zro2 using a diamond anvil and single crystal x-ray diffraction method, Phys. Chem. Miner. **13**, 233 (1986).

[66] O. Ohtaka, T. Yamanaka, S. Kume, N. Hara, H. Asano, and F. Izumi, Structural analysis of orthorhombic ZrO_2 by high resolution neutron powder diffraction, Proc. Jpn. Acad., Ser. B **66**, 193 (1990).

[67] J. Haines, J. M. Léger, S. Hull, J. P. Petitet, A. S. Pereira, C. A. Perottoni, and J. A. H. da Jornada, Characterization of the cotunnite-type phases of zirconia and hafnia by neutron diffraction and Raman spectroscopy, J. Am. Ceram. Soc. **80**, 1910 (1997).

[68] https://www.gauss-centre.eu/.

[69] https://www.lrz.de.